Title

Pyrimidine starvation activates a bistable phenotypic switch leading to ribosome provisioning and rapid exit from stationary phase

Authors:

P. Remigi[1], G.C. Ferguson[2], S. De Monte[3] and P.B. Rainey[1,4,5]

[1] New Zealand Institute for Advanced Study, Massey University, Auckland 0745, New Zealand

[2] Institute of Natural and Mathematical Sciences, Massey University, Auckland 0745, New Zealand

[3] Institut de Biologie de l'Ecole Normale Superieure, UMR CNRS 8197 INSERM 1024, F-75005 Paris, France

[4] Department of Microbial Population Biology, Max Planck Institute for Evolutionary Biology, Plön 24306, Germany

[5] Ecole Superieure de Physique et de Chimie Industrielles de la Ville de Paris (ESPCI Paris Tech), CNRS UMR 8231, PSL Research University, 75231 Paris, France

Corresponding authors:

Philippe Remigi (p.remigi@massey.ac.nz) and Paul B. Rainey (rainey@evolbio.mpg.de)

Abstract:

Observations of bacteria at the single-cell level have revealed many instances of phenotypic heterogeneity within otherwise clonal populations, but the selective causes, molecular bases and broader ecological relevance remain poorly understood. In an earlier experiment in which the bacterium *Pseudomonas fluorescens* SBW25 was propagated under a selective regime that mimicked the host immune response, a genotype evolved that stochastically switched between capsulation states. The genetic cause was a mutation in *carB* that decreased the pyrimidine pool (and growth rate) lowering the activation threshold of a pre-existing but hitherto unrecognised phenotypic switch. Genetic components surrounding bifurcation of UTP flux towards DNA/RNA or UDP-glucose (a precursor of colanic acid forming the capsules) were implicated as key components. Extending these molecular analyses – and based on a combination of genetics, transcriptomics, biochemistry and mathematical modelling – we show that pyrimidine limitation triggers an increase in ribosome biosynthesis and that switching is caused by competition between ribosomes and CsrA/RsmA proteins for the mRNA transcript of a feed-forward regulator of colanic acid biosynthesis. We additionally show that in the ancestral bacterium the switch is part of a programme that determines stochastic entry into the semi-quiescent capsulated state, ensures that such cells are provisioned with excess ribosomes, and enables provisioned cells to exit rapidly from stationary phase under permissive conditions.

39 **Introduction:**

40 Phenotypic variation between isogenic cells growing in homogeneous environments can have
41 adaptive consequences, allowing populations to survive unpredictable environmental changes or
42 promoting interactions between different cell types (ACKERMANN 2015; VAN BOXTEL *et al.* 2017).
43 Natural selection, by means of genetic mutations affecting the integration of stochastic noise within
44 signaling pathways, can fine-tune epigenetic switches (ROTEM *et al.* 2010; FRIDMAN *et al.* 2014; NEW *et*
45 *al.* 2014; RICHARD AND YVERT 2014; VAN DEN BERGH *et al.* 2016; BODI *et al.* 2017) but the molecular
46 details underpinning the evolution of phenotypic heterogeneity remain poorly understood.

47 An opportunity to study the genetic bases of the evolution of phenotypic heterogeneity arose from a
48 selection experiment where the capacity to switch between different colony phenotypes evolved *de*
49 *novo* in the bacterium *Pseudomonas fluorescens* SBW25 (BEAUMONT *et al.* 2009). In this experiment,
50 bacteria were passaged through consecutive cycles comprised of single-cell bottlenecks and negative
51 frequency-dependent selection, a regime mimicking essential features of the adaptive immune
52 system in animals. A strain emerged (1B4) that forms distinct opaque or translucent colonies on agar
53 plates. At the single-cell level, this behaviour reflects an epigenetic switch characterized by the
54 bistable production of an extracellular capsule, resulting in the coexistence of two sub-populations
55 of capsulated (Cap+) or non-capsulated (Cap-) cells. Capsules are made of a colanic acid-like
56 polymer, whose production arises from the activity of the *wcaJ-wzb* locus and requires the precursor
57 UDP-glucose. A mutation in *carB*, a gene involved in *de novo* pyrimidine biosynthesis, is responsible
58 for heterogeneous capsule production via a decrease in intracellular pyrimidine pools (BEAUMONT *et*
59 *al.* 2009; GALLIE *et al.* 2015). Additionally, the switch between capsulated and uncapsulated cells was
60 shown to function in the ancestral gentoype devoid of the *carB* mutation – the *carB* mutation having
61 altered the threshold at which the switch is activated – and underpins the stochastic entry of cells
62 into a semi-quiescent state.

63 Here we extend earlier work and present a detailed mechanistic model that explains how the *carB*
64 mutation impacts on capsulation heterogeneity. Central to the model is evidence that ribosome
65 biosynthesis is up-regulated upon pyrimidine limitation and that this favors translation of a positively
66 auto-regulated activator of capsular exopolysaccharide biosynthesis that is otherwise inhibited by
67 CsrA/Rsm proteins. The switch comprises part of a programme that facilitates stochastic entry into a
68 semi-quiescent state and rapid exit from this state upon realisation of permissive conditions through
69 modulation of ribosome levels.

70

71

72 **Results**

73 **Capsulation is not induced by UDP-glucose depletion**

74 The paradoxical observation that pyrimidine limitation induced capsulation, a phenotypic trait
75 depleting the pyrimidine pool even more through the consumption of UDP-glucose, caused
76 attention to focus on the link between capsulation, growth and pyrimidine metabolism (GALLIE *et al.*
77 2015). In particular, the fact that capsulation may represent a semi-quiescent state whose initiation
78 is triggered by fluctuations in the concentration of an intermediate of the pyrimdine biosynthetic
79 pathway suggested that this metabolite may act both as a signal for capsulation and as a cell cycle
80 checkpoint. UDP-glucose appeared a prime candidate for this function, since it is a widely conserved
81 signal regulating cell size and bacterial growth (VADIA AND LEVIN 2015). A transposon insertion in *galU*
82 (encoding the enzyme required for UDP-glucose biosynthesis) prevented capsulation (GALLIE *et al.*
83 2015), but a role for UDP-glucose as a building block for colanic acid or as a signal for its activation
84 remained undetermined. Introduction of a translational reporter of capsulation in the *galU* mutant
85 (with undetectable UDP-glucose levels; GALLIE *et al.* 2015) revealed that the proportion of cells
86 expressing this reporter was lower in the mutant compared to 1B4 (Supplementary Figure 1). This is
87 in contrast to the predicted response if a reduction in the concentration of UDP-glucose was the
88 signal inducing capsulation. This key result caused us to revisit the mechanistic links between
89 pyrimidine limitation, growth rate and the heterogeneous production of colanic acid capsules.

90

91 **Ribosomes are over-produced in *carB* mutants**

92 We re-analysed transcriptomic data (published in GALLIE *et al.* 2015) to identify signalling pathways
93 that may display different levels of activity as a result of the *carB* mutation. KEGG-enrichment
94 analyses showed over-representation of ribosomal components among the genes that are expressed
95 at least two-fold more in the capsulated sub-population of 1B4 (1B4 Cap+) compared to its (non-
96 capsulated) ancestor 1A4 (Supplementary Table 1). By extracting raw expression values from the
97 available RNAseq datasets, we observed that the average expression levels of ribosomal protein
98 genes increase in 1B4 (either Cap- or Cap+) compared to 1A4 or SBW25 (Fig. 1a). Such a finding is
99 surprising since ribosome production is usually proportional to growth rate (DENNIS *et al.* 2004; PAUL
100 *et al.* 2004) and was expected to be reduced in the slower growing strain 1B4 (Supplementary Figure
101 2).

102 In bacteria, correct adjustment of ribosomal production to nutrient availability is essential to
103 maximise growth rate. Bacteria do so by modulating transcriptional activity at the promoters of

104 ribosomal RNA (*rrn*) operons (DENNIS *et al.* 2004; PAUL *et al.* 2004). The production of ribosomal
105 proteins is then adjusted to the level of available rRNA (KEENER AND NOMURA 1996). The over-
106 expression of ribosomal protein genes in 1B4 may therefore reflect transcriptional up-regulation at
107 *rrn* promoters. Using a chromosomally-integrated reporter, an increase in P*rrnB*-GFP transcriptional
108 activity was detected in *carB* mutants compared to immediate ancestral types (Fig. 1b). This
109 difference was most obvious when cultures reached OD~2, a density at which 1B4 cultures undergo
110 a noticeable increase in capsulation (Supplementary Figure 3). Supplementing growth media with
111 2mM uracil – a treatment known to suppress capsulation (GALLIE *et al.* 2015) – restored wild-type
112 P*rrnB*-GFP expression in strains carrying the mutant *carB* allele (Fig. 1b). Together with the higher
113 total RNA concentration measured in *carB* mutants (Fig. 1c), these results show that pyrimidine
114 limitation triggers the production of an enhanced pool of active ribosomes.

115

116 **High ribosome levels are required for capsulation**

117 The counterintuitive effect of the mutation in *carB* on ribosome levels suggested a causal connection
118 between ribosome concentration and capsulation. In support of this hypothesis, a previous
119 transposon-mutagenesis screen found that insertions in ribosome- or translation-associated genes
120 (*prfC, rluB, rluC, glu/gly* tRNA) decreased or abolished capsulation in 1B4 (GALLIE *et al.* 2015). We set
121 out to manipulate ribosome concentration in 1B4 in order to test directly if ribosome abundance has
122 an impact on capsulation. *P. fluorescens* SBW25 harbours 5 *rrn* copies (*rrnA-E*) and, in bacteria, the
123 deletion of a single operon can often be compensated for by the over-expression of those remaining
124 (CONDON *et al.* 1993; BOLLENBACH *et al.* 2009; GYORFY *et al.* 2015). Capsulation was quantified in single
125 or double *rrn* deletion mutants carrying the chromosomally-inserted translational reporter
126 P*pflu3655*-GFP (Gallie *et al*., 2015) by measuring the proportion of GFP positive cells in cultures at
127 the onset of stationary phase (OD~2). Whereas single mutants were not significantly affected in their
128 capsulation levels, double mutants produced fewer capsulated cells (Fig. 2a and Supplementary
129 Figure 4). A reduction in RNA concentration (Supplementary Figure 5) was observed in the *rrnAE*
130 double mutant, but not in *rrnAC* that showed a milder capsulation phenotype. Together, these
131 results show that capsulation is induced by increased ribosome dosage, which is itself a consequence
132 of the *carB* mutation.

133

134 **A ribosome-Rsm competition model for the control of capsulation**

135 Next, we asked how ribosome abundance may influence the heterogeneous production of
136 capsulated cells in an isogenic population. Results from a previous transposon mutagenesis screen
137 indicated that the Gac/Rsm two-component signalling pathway is required for the production of
138 colanic acid-like capsules (GALLIE *et al.* 2015) . The Gac/Rsm signalling pathway controls important
139 ecological traits in many Gram-negative bacteria (VAKULSKAS *et al.* 2015; VALENTINI *et al.* 2017). Its
140 activity is mediated through post-transcriptional regulators of the Csr/Rsm family that can prevent
141 translation of mRNA targets by binding sites adjacent to or overlapping ribosome-binding sites (RBS)
142 (LAPOUGE *et al.* 2008; VAKULSKAS *et al.* 2015). The phenotypic effect of the Gac/Rsm pathway was
143 investigated by creating deletion mutants for the response regulator *gacA* and the two Csr/Rsm
144 homologs present in SBW25, namely *rsmA* and *rsmE.* Capsulation was completely abolished in the
145 *gacA* deletion strain, confirming the transposon-mutagenesis results (Fig. 2b). Deletion of *rsmA* or
146 *rsmE* increased the production of capsulated cells, consistent with their typical inhibitory role in
147 Gac/Rsm signalling pathways.

148 We postulated that variations in the relative concentration of free ribosomes and RsmA/E may
149 determine translational output of a key positive regulator of capsule biosynthesis (Fig. 2c). While
150 searching for such a regulator, attention turned to *PFLU3655*. The first gene of a putative operon
151 (*PFLU3655-3657*) localized just upstream of the colanic acid biosynthetic operon, *PFLU3655* is
152 annotated as a hypothetical protein carrying a two-component response regulator C-terminal
153 domain (PFAM PF00486). *PFLU3655* is among the most highly up-regulated genes in 1B4 Cap+ cells
154 and transposon insertions in its promoter were shown to abolish capsulation in 1B4 (GALLIE *et al.*
155 2015). A non-polar deletion of *PFLU3655* in 1B4 abolished capsule formation, while
156 complementation of the mutant with an IPTG-inducible copy of *PFLU3655* on a low copy number
157 plasmid (pME6032) restored capsulation (Fig. 3a). Over-expression of *PFLU3655* in SBW25 or 1B4
158 was sufficient to induce high capsulation levels in these strains, showing that PFLU3655 is a key
159 positive regulator of colanic acid biosynthesis, the expression of which is necessary and sufficient for
160 capsulation. Moreover, expression of PFLU3655 is also necessary and sufficient to induce the
161 expression of its own promoter, as measured with the chromosomally-encoded P*pflu3655*-GFP
162 translational fusion (Fig. 3b). This result shows that PFLU3655 expression can generate a positive
163 feedback loop, a motif that can sustain bistable gene expression (VEENING *et al.* 2008; NORMAN *et al.*
164 2015).

165

166 **Ribosome-Rsm interaction at the PFLU3655 promoter**

167 Existence of a positive fedback loop does not warrant bistability, which often requires the additional
168 presence of an ultrasensitive switch to convert small input deviations (typically, molecular noise)
169 into large output differences (FERRELL AND HA 2014). When signalling components are present in large
170 numbers, ultrasensitive responses and threshold effects can arise through molecular titration where
171 a molecule (RNA or protein) is sequestered and inhibited by another protein (BUCHLER AND LOUIS
172 2008; BUCHLER AND CROSS 2009; FERRELL AND HA 2014).

173 The possibility that titration of a target mRNA by RsmA/E may trigger ultrasensitivity was considered.
174 Interestingly, two putative Rsm binding sites are located in the promoter and 5' region of the coding
175 sequence of *PFLU3655* (Fig. 4a), indicating that PFLU3655 mRNA could be a direct target of RsmA/E.
176 The P*pflu3655*-GFP capsulation reporter was used to test this hypothesis. This translational reporter
177 contains ~500 nucleotides upstream of PFLU3655 start codon and the first 39 coding nucleotides
178 fused to GFP in frame; the two putative RsmA/E binding sites are conserved in this synthetic
179 construct. Using site-directed mutagenesis, nucleotides located in the putative Rsm binding sites
180 were substituted and effects on GFP production in the P*pflu3655*-GFP reporter determined (Fig.
181 4a,b). Both G-8A and A33T point mutations increased GFP production, albeit to a different extent,
182 consistent with the expected effects arising from reduction in binding of an inhibitor. Altering the
183 putative RBS (GG-7AC) completely abolished GFP production (Fig. 4b), which is similarly to be
184 expected given the need for translation. Re-introducing these point mutations at the original locus in
185 1B4 showed that the G-8A mutation, but not the A33T, increased the proportion of capsulated cells
186 (Fig. 4c). This difference mirrors the extent of presumed translational mis-regulation by the two
187 point mutations and suggests that the increase in PFLU3655 translation mediated by the A33T
188 mutation is not sufficient to increase the likelihood to jump-start the positive feedback loop,
189 contrary to G-8A.

190 Together, these data support the model proposed earlier (Fig. 2c). If this model is correct, one would
191 expect other RsmA/E targets to be over-expressed in *carB* mutants. To this end, a list of genes that
192 were differentially expressed in a SBW25 *gacS* mutant (CHENG *et al.* 2013) was extracted and their
193 expression levels were compared using the RNAseq dataset. On average, genes that were up-
194 regulated in the *gacS* mutant were expressed at lower levels in 1B4 (both Cap- and Cap+) than in
195 SBW25 or 1A4 (Supplementary Figure 6). Genes that were down-regulated in *gacS* showed a slight
196 bias towards higher expression in 1B4 Cap+ but this difference was not statistically significant. These
197 results are consistent with the opposing effects of *gacS* inactivation (leading to constitutive
198 activation of RsmA/E) and *carB*-dependent increase in ribosome concentration on RsmA/E targets.

199

200 **A qualitative mathematical model of the genetic network controlling bistable capsule production**
201 **explains experimental results**

202 We produced a mathematical model based on our experimental observations in order to describe
203 the qualitative behaviour of the cells, notably the bistability of the internal state, and to predict how
204 changes in parameters are likely to affect the fraction of capsulated cells.

205 The abundance of PFLU3655, represented by the variable x, is described by the following ordinary
206 differential equation:

$$\frac{dx}{dt} = P(x) - dx$$

207 where P(x) is the production rate and the constant d measures the rate of degradation/dilution (or
208 decay) per molecule. The existence of a positive feedback loop in PFLU3655 production and the
209 plausible assumption that RsmA/E and ribosome compete to bind *PFLU3655* mRNA led us to choose
210 an ultrasensitive curve for the production term P(x) (Fig. 5a; see Supplementary text for full details
211 on the model), analogous to other cases of molecular titration (BUCHLER AND LOUIS 2008; BUCHLER AND
212 CROSS 2009; ZHANG *et al.* 2013). For fixed concentrations of RsmA/E and ribosomes, the shape of this
213 curve is characterized by a nonlinear increase of production with x. For low x, even though *PFLU3655*
214 is transcribed proportionally to x, sequestration of its mRNA by RsmA/E maintains translation, thus
215 the concentration of the protein, at low levels. When the number of mRNA molecules exceeds the
216 buffering capacity of the RsmA/E pool, then translation increases massively, but it eventually
217 saturates for high values of x, due to the competition for the ribosome pool.

218 The equilibrium solutions of the system x_E are found when the production equalizes the decay
219 ($P(x_E)= d\ x_E$). When the decay term is sufficiently small (dashed purple line in Fig. 5a), the system is
220 bistable, with two stable (corresponding to the OFF (x_E=0) and the ON ($x_E=x^{on}$) states) and one
221 unstable ($x_E=x^S$) equilibria. The unstable solution separates the space of concentrations x in two
222 basins of attraction of the stable equilibria. Stochastic fluctuations in the components of the system
223 can activate or inactivate capsulation by letting x change the basin of attraction and subsequently
224 approach the corresponding equilibrium. The smaller the basin of attraction of the OFF equilibrium,
225 (smaller x^S) the higher the probability that random fluctuations cause the system to switch to the ON
226 state, and vice-versa. Thus, the position of x^S defines the proportion of cells found in the capsulated
227 ON state.

228 Qualitative changes in the behaviour of the system can be explored by a graphical analysis of the
229 equilibria. An increase in ribosome concentration leads to an increase in the maximal production
230 rate P(x), which can be sufficient to generate bistability (Fig. 5b, blue line). Starting from a bistable

231 situation (blue line), the probability of switching ON can be enhanced through an increase of the
232 basal production rate of PFLU3655 (Fig. 5c**,** light blue line). These observations qualitatively match
233 experimental results previously described (Fig. 3), indicating that this simple model encapsulates
234 fundamental aspects of the switching mechanism.

235 **Consequences of ribosome accumulation on growth resumption in capsulated cells**

236 A corollary of our model is that, if ribosome levels fluctuate between isogenic cells, cells with highest
237 ribosome concentrations should be more likely to produce capsules. Indeed, RNAseq data indicate
238 that ribosomal protein genes are expressed at higher levels in 1B4 cap+ compared to 1B4 cap- (Fig.
239 1a). When the quality and/or quantity of nutrients rises abruputly, differences in ribosome
240 abundance can be significant for bacterial fitness (MORI *et al.* 2017). Reaching higher ribosome
241 concentration – required for maximal growth rate after nutrient up-shift – is time-consuming and
242 means a time-delay between environment change and future growth (EHRENBERG *et al.* 2013). Cells
243 with higher ribosome concentrations before nutrient up-shift might be considered as provisioned for
244 rapid acclimation to the new conditions. If it is true that (i) capsulated cells have more ribosomes
245 and (ii) ribosomes promote growth resumption after nutrient up-shift, then capsulated cells should
246 have a fitness advantage in those conditions. To test this prediction, 1B4 cells grown to late
247 exponential phase (OD_{600nm}~1) and cell suspensions enriched in Cap- or Cap+ cells were used to
248 inoculate fresh cultures. The initial growth rate after nutrient up-shift in batch cultures was
249 positively correlated with the proportion of capsulated cells (Fig. 6a). Time-lapse microscopy on solid
250 agar pads confirmed that colonies founded by GFP+ (capsulated) cells grew approximately 10%
251 faster than those originating from GFP- (non-capsulated) cells (Fig. 6b).

252

253 **Capsulation in SBW25**

254 The identification of mechanisms promoting the production of colanic acid capsules in evolved
255 *P. fluorescens* genotypes raises questions as to the role and conditions for expression of colanic acid
256 in ancestral SBW25. In bacteria, extracellular capsules are important for bacterial pathogenicity
257 (ROBERTS 1996) and are associated with broader environmental versatility (RENDUELES *et al.* 2017).
258 Recent work has also demonstrated a role for colanic acid-like capsules in the positioning of the cells
259 at the surface of bacterial colonies, providing them with a better access to oxygen and a fitness
260 advantage (KIM *et al.* 2014; KIM *et al.* 2016).

261 In order to test if capsulation could occur in wild-type SBW25 colonies, we spot-inoculated bacterial
262 suspensions on agar plates and incubated the plates at 28°C for several days. Mucoid swellings were

263 observed from 5 days post-inoculation and increased over time (Fig. 7a). These swellings were not
264 observed with a colanic acid mutant and their appearance was delayed when 2mM uracil was added
265 to agar plates (Fig. 7b). In SBW25, cells sampled from mucoid regions showed a high proportion of
266 capsulated cells, approximately 60% of which expressed the Ppflu3655-GFP reporter (Fig 7c).
267 However, when streaked on new agar plates, no phenotypic difference was observed between cells
268 coming from these mucoid areas and regular SBW25 colonies (data not shown), indicating that
269 mucoidy was not dependent on *de novo* mutation. These results are in accord with predictions and
270 indicate that capsulation in starved SBW25 colonies is also a consequence of bistable colanic acid
271 production resulting from nutrient limitation.

272 Given previous results with 1B4, the possibility arose that capsulated SBW25 cells might also benefit
273 from a growth advantage upon exposure to rich medium. Cells were collected from 7-day old
274 colonies and enriched in capsulated or non-capsulated cells by gentle centrifugation. When
275 transfered to fresh batch cultures, cell suspensions enriched in capsulated cells showed a faster
276 initial growth rate (Supplementary Figure 7) that resulted in a fitness advantage during head-to-head
277 competition (Fig. 7d). Moreover, time-lapse microscopy revealed that micro-colonies founded by
278 GFP+ cells display an initial growth rate significantly higher than colonies arising from GFP- cells (Fig
279 7e).

280 To test if capsulation status in SBW25 is also associated with higher ribosome content, we measured
281 expression of the ribosomal protein gene *rpsL* in capsulated and non-capsulated cells originating
282 from old SBW25 colonies by RT-qPCR. We found an expression ratio of 1.67 (+/- 0.35 s.d., n=5, two-
283 tailed t-test: p=0.012) in cap+ vs. cap- cells, suggesting that SBW25 capsulated cells contain more
284 ribosomes than their non-capsulated counter-parts.

285 Overall, the results from experiments carried out in SBW25 are consistent with the capsulation
286 model proposed for 1B4. During 'long-term' (*i.e.*, 7 days) starvation, nutrient limitation (possibly flux
287 through the pyrimidine pathway and likely associated with spatial heterogeneity within colonies)
288 establishes a sub-population of cells with increased ribosome content. This population then has an
289 enhanced chance of flipping to the capsulated state where growth remains slow and cells enter a
290 semi-quiescent state. This same sub-population then stands primed for rapid growth upon nutrient
291 upshift.

292

293

294

295 **Discussion:**

296 Studies of adaptive phenotypes derived from selection experiments are by nature multifaceted, but
297 two parallel lines of inquiry are of particular importance. The first concerns the nature of the
298 adaptive phenotype, including its selective and molecular causes. The second concerns the
299 ecological significance of the traits affected by adaptive evolution, prior to the occurrence of the
300 adaptive mutation(s). A satisfactory answer to the first requires understanding of the latter.

301 Consider initial discovery of the 1B4 switching genotype (BEAUMONT *et al.* 2009): a remarkable
302 behaviour that owes its existence to reduction of function of carbamoyl phosphate synthase (GALLIE
303 *et al.* 2015). In and of itself discovery of the causal switch-generating mutation shed no light on the
304 adpative phenotype. Understanding began to emerge upon recognition that the *carB* mutation had
305 altered the activation threshold of a pre-existing switch.

306 Here we have substantially extended understanding of both the mechanistic bases of phenoytpic
307 switching in the derived 1B4 genotype, and also the ecological significance of the underlying traits in
308 the ancestral genotype. The former is specific to the selection experiment, whereas the latter has
309 likely relevance of a more general nature. Indeed, as is often the case, studies of phenotypes derived
310 from in vitro selection experiments can shed light on hitherto unrecognised aspects of bacterial
311 physiology (HINDRE *et al.* 2012; RAINEY *et al.* 2017; and references therein).

312 With attention on the mechanistic basis of the 1B4 switch, experiments examining function of the
313 switch in a *galU* mutant showed that the previous conclusions concerning the central role of UTP or
314 related molecules required revision. While pyrimidine biosynthesis and the UTP decision point are
315 important components of the pathways leading to capsulation, the mechanism of switching resides
316 elsewhere. Data presented here have led to formulation of a compelling new model of the switch.
317 Central to the proposed model (Fig. 2c) is titration of *PFLU3655* mRNA by RsmA/E that has the
318 potential to generate an ultrasensitive response. The increase in ribosome production resulting from
319 the *carB* mutation brings the system closer to its activation threshold, where small fluctuations in
320 ribosome and/or in RsmA/E activities initiate a positive feedback loop leading to capsulation. Given
321 the prevalence of inhibitory interactions in signaling networks, pathways with these features offer a
322 common route for the evolution of or evolutionary tuning of bistable switches through relatively
323 minor changes to the basal level (or interaction affinity) of threshold-defining components (BUCHLER
324 AND CROSS 2009; ROTEM *et al.* 2010).

325 Data supporting this revised model comes largely from experiments described here, but also
326 incorporates data presented in Gallie *et al.* (2015) that at the time were inexplicable. Most notably

327 data indicating a role for ribosomes, which stemmed from transcriptome data, but also from analysis
328 of mutants defective in switching obtained from the original suppressor study. Here numerous non-
329 switching types carried transposon insertions in genes implicated in ribosome or translation-
330 associated activities. Additional mutants that remained unincorporated included that Gac pathway
331 and its connection to RsmA/E and the newly recognised regulator of colanic-acid production
332 (PFLU3655).

333 Understanding the switch requires understsanding of its role in the ancestral genotype. Previous
334 work showed that switching to the capsulated type was accompanied by a reduction in growth rate.
335 This work also showed that the probability of switching to the capsulated state was more likely in
336 starved cells (particularly in cells starved of pyrimidines). This was understood as a mechanism that
337 allowed cells entering starvation conditions to hedge their bets in the face of uncertainty
338 surrounding the future state of the environment (GALLIE *et al.* 2015). Discovery (from this work) that
339 capsulated cells, despite slow growth, are replete in ribosomes was perplexing, but caused attention
340 to focus on exit from the semi-quiescent state. Just as cells entering a slow growing phase stand to
341 be out-competed by conspecific types that remain in the active growth phase if the environment
342 unexpectedly returns to one conducive for growth, cells exiting from a slow growth state stand to be
343 out-competed by types that are already actively growing unless they can rapdily resume "life in the
344 fast lane".

345 Although the subject of little attention in the microbiological world (but see (MORI *et al.* 2017) and
346 below), the importance of provisioning future generations with resources sufficient to aid
347 estabishment is a central part of life-history evolution theory (STEARNS 1992). It is not difficult to
348 conceive that cells entering a slow or non-growing state, such as persistors, or the capsulated cells of
349 SBW25, will through evolutionary time, experience selection for mechanisms that facilitate rapid re-
350 entry to active growth. Our data here is strongly indicative of such an evolutionary response.

351 Nutrient starvation leads to stochastic activation of capsulation and entry into a semi-quiescent
352 growth phase. At the same time such capsulated cells contain above average concentrations of
353 ribosomes. Upon encountering conditions conducive for growth capsulated cells rapidly switch to
354 the non-capsulated state (GALLIE *et al.* 2015), but remarkably, out-compete non-capsulated cells. A
355 phenomenom of ribosome over-capacity that bears similarity to what we have interpreted as
356 'ribosome provisioning', was described previously in fast growing bacteria (KOCH 1971): production
357 of excess ribosomes during exponential growth, while being deleterious in the short term, can
358 provide an advantage during nutrient up-shift (MORI *et al.* 2017). In environments where resource
359 availability fluctuates, it appears that the control of ribosome biosynthesis might be subjected to a

360 trade-off between maximising growth rate before starvation and growth resumption upon nutrient
361 up-shift (MORI *et al.* 2017). Our findings add a single-cell perspective showing that cell-to-cell
362 heterogeneity in ribosome activity during stationary phase may contribute to maximisation of long-
363 term geometric mean fitness.

364

365

366 **Material and methods:**

367

368 *Bacterial strains and growth conditions*

369 Bacterial strains used in this study are listed in Supplementary Table 2. Unless otherwise stated,
370 *Pseudomonas fluorescens* strains were cultivated in King's Medium B (KB; KING *et al.* 1954)) at 28°C
371 with orbital shaking. *Escherichia coli* DH5α λ*pir* was used for clonings and was grown on Lysogeny
372 Broth at 37°C. Bacteria were plated on their respective growth medium containing 1.5% agar.
373 Antibiotics were used at the following concentrations: ampicillin (50-100 µg mL^{-1}), gentamicin (10 µg
374 mL^{-1}), tetracycline (10 µg mL^{-1}), kanamycin (25 or 50 µg mL^{-1} for *E. coli* or *P. fluorescens*, respectively)
375 and nitrofuorantoin (100 µg mL^{-1}). Uracil (Sigma-Aldrich) was added to culture medium at 2mM final
376 concentration when indicated. For competition experiments, 5-bromo-4-chloro-3-indolyl-β -d-
377 galactopyranoside (X-gal) was used at a concentration of 60 mg L^{-1} in agar plates.

378 For capsulation assays, pre-cultures were inoculated from pre-calibrated dilutions of frozen glycerol
379 aliquots in order to reach an optical density of 0.3-0.5 after overnight culture.

380 For colony assays with SBW25, 5µl of cell suspensions were spot-inoculated on KB agar plates and
381 incubated for 7 days at 28°C. Cells from the center of these colonies were resuspended in PBS or
382 Ringer's solution for growth and competition assays and time-lapse microscopy, or in RNAlater
383 solution (Invitrogen) for RT-qPCR.

384

385 *Molecular techniques*

386 Oligonucleotides and plasmids used in this study are listed in Supplementary Tables 3 and 4,
387 respectively. Standard molecular biology techniques were used for DNA manipulations (SAMBROOK *et*
388 *al.* 1989). DNA fragments used to generate promoter fusions and gene deletion constructs were
389 prepared by splicing by overhang extension polymerase chain reaction (SOE-PCR; HO *et al.* 1989). All

390 DNA fragments generated by SOE-PCR were first cloned into the pGEM-T easy vector (Promega) and
391 their fidelity was verified by Sanger sequencing (Macrogen, Seoul, South-Korea). Plasmids were
392 introduced into *P. fluorescens* by tri-parental conjugations with the helper plasmid pRK2013,
393 carrying the *tra* and *mob* genes required for conjugation. Tn7-based plasmids were mobilized into
394 recipient strains with the additional helper plasmid pUX-BF13 (BAO *et al.* 1991).

395 To generate deletion mutants (*rrn* operons, *gacA, rsmA, rsmE* and *pflu3655*), regions flanking the
396 genes or operons of interest were amplified from SBW25 genomic DNA and assembled by SOE-PCR.
397 Deletion cassettes were inserted into the pUIC3 plasmid (RAINEY 1999) as SpeI fragments and
398 mutants were obtained following the two-step allelic exchange protocol described previously (ZHANG
399 AND RAINEY 2007). Deletion mutants were checked by PCR. To check *rrn* copy number after *rrn*
400 deletions, quantitative PCR were performed using a protocol described previously (FARR *et al.* 2017).

401 For complementation and over-expression studies, *PFLU3655* was amplified with oPR206/oPR207
402 and cloned into pME6032 (HEEB *et al.* 2002) as *EcoR*I/*Xho*I restriction fragment, downstream of the
403 P*tac* promoter.

404 To generate the Tn7-P*rrnB*-GFP reporter, a ~600bp fragment upstream of the *rrnB* operon (*PFLUr7-*
405 *11*) was amplified from SBW25 genomic DNA (oPR148/oPR151) and fused by SOE-PCR to *gfp-mut3.1*
406 sequence containing the T0 terminator previously amplified with oPR152/FluomarkerP2 from the
407 miniTn7(Gm)-P*rrnB1-gfp-a* plasmid (Lambertsen *et al.* 2003). The resulting fragment was cloned into
408 pUC18R6K-miniTn7T-Gm (CHOI *et al.* 2005) as a *Spe*I restriction fragment.

409 Site-directed mutagenesis of putative RsmA/E binding sites in pGEMTeasy-P*pflu3655*-GFP plasmid
410 was performed using the Quick Change mutagenesis kit (Stratagene) according to manufacturer's
411 instructions. Mutagenized fragments were then cloned into pUC18R6K-miniTn7T-Gm (CHOI *et al.*
412 2005) as a *Spe*I restriction fragment. In order to re-engineer point mutations in RsmA/E into
413 *Pseudomonas fluorescens* genome, a 1.5kb fragment spanning equal length on each site of the
414 target sites was amplified with oPR37/oPR223 and cloned into pGEM-T easy vector. Site-directed
415 mutagenesis was performed on this plasmid as described above, and the resulting DNA fragments
416 were cloned in pUIC3 as *Spe*I restriction fragments and introduced into *P. fluorescens* genome by
417 double recombination.

418

419 *RNA extractions and RT-qPCR*

420 For quantification of RNA concentration in bacterial cultures, cells were harvested from 1ml of
421 cultures at OD 0.5-1 and resuspended in 200ul of RNAlater solution (Invitrogen). For total RNA

422 quantification, we followed the method described by You *et al.* (2013), except that, before
423 processing, cells cultures were resuspended in RNAlater (Invitrogen) instead of being fast frozen on
424 dry ice. To normalise total RNA concentrations, the relationship between cell density and OD_{600nm}
425 was established for each strain by counting cells with a hemocytometer in 5 independent cultures of
426 similar OD to those used for RNA extractions.

427 Reverse-transcription quantitative PCR were performed as described previously (FARR *et al.* 2017),
428 using *gyrA* as an internal control. Oligonucleotide primers used for RT-qPCR are listed in
429 Supplementary Table 3.

430

431 *Capsulation and gene expression assays*

432 For capsulation test, cells were grown from standardized glycerol aliquots stored at -80°C. Aliquots
433 were diluted in KB and pre-cultures were grown overnight in order to reach an OD ~0.3-0.5 in the
434 morning. For gene expression studies, overnight pre-cultures were grown to saturation. In both
435 cases, pre-cultures were diluted to OD_{600nm}=0.05 in KB and incubated at 28°C. IPTG was added to a
436 final concentration of 0.1-1mM when indicated. Samples were taken at different time points for flow
437 cytometry and OD measurements. GFP fluorescence in bacterial populations was measured with a
438 BD FACS Canto II flow cytometer. Cell suspensions were diluted to a density of ~ 10^5 cells ml^{-1} in
439 filter-sterilised PBS and at least 20,000 cells were analysed by flow cytometry. Cellular debris were
440 filtered using side- and forward-scatter channels. GFP fluorescence was detected with a 488 nm
441 laser with 530/30 bandwidth filter. Laser intensity was set to 600V, except for P*rrnB*-GFP analyses
442 where intensity was lowered to 300V. Flow cytometry data files were analysed in R using the
443 flowCore package (ELLIS *et al.* 2017).

444

445 *Growth curves in microplate reader*

446 Overnight precultures were adjusted to OD_{600nm}=0.05 in fresh KB and used to start growth curves in a
447 Synergy 2 microplate reader (Biotek) in 96-well plates. Cultures were incubated for at least 24h at
448 28C with constant shaking and OD_{600nm} was read every 5 minutes.

449 To measure growth rates of cultures enriched in capsulated or non-capsulated cells, cells were
450 harvested from late-exponential phase (OD_{600nm}~1; 1B4) or 7-day old colonies (SBW25) and
451 centrifuged (1 min, 3000 rpm). Supernatants and pellets were collected, representing sub-
452 populations enriched in capsulated and non-capsulated cells, respectively. Cell suspension density

453 was adjusted to OD_{600nm}=0.05 in KB to start growth curves. Initial growth rates were calculated by
454 performing a linear regression on the logarithm of the measure OD values during the first 2h of
455 growth. Slopes of these linear regressions are reported as growth rate values.

456

457 *Microscopy*

458 Indian ink staining of capsulated cells was performed as described previously (GALLIE *et al.* 2015). For
459 time-lapse microscopy, bacteria were harvested from late exponential phase (1B4, OD~1-2) or from
460 7 day-old colonies (SBW25), diluted 1:1000 in KB and 2µl of the resulting suspension was
461 immediately transferred on a gel pad (1% agar KB) located on a glass slide within an adhesive frame
462 (GeneFrame, Thermo-Fisher). When dry, a cross-section of the pad was removed with a razor blade
463 in order to allow gaz exchanges to occur, the preparation was sealed with a glass cover-slip and
464 transferred to the microscope incubation chamber pre-heated at 28°C. Time lapse microscopy
465 experiments was performed with an Olympus BX61 upright microscope equipped with an F-View II
466 monochrome camera, a motorized stage and a temperature-controlled chamber set at 28°C. Devices
467 were operated by the Olympus Cell^P or CellSens softwares. Phase-contrast images were acquired
468 every 10 minutes with an oil-immersion 100x objective. One GFP image was taken before starting
469 the experiment in order to determine the capsulation status of each cell.

470 Phase contrast images were segmented with Fiji (SCHINDELIN *et al.* 2012) and individual colony areas
471 were extracted. For each colony analysed, the capsulation status of founding cell was scored
472 manually. The logarithm of the growth rate of individual 1B4 colonies was then fitted using a linear
473 regression. For SBW25, segmented linear regressions were found to better fit the data and the slope
474 of the first line was reported.

475

476 *RNAseq analyses*

477 RNAseq data were published previously (GALLIE *et al.* 2015). KEGG orthology terms for SBW25
478 genome were downloaded from the KEGG Orthology database (www.genome.jp; accessed in April
479 2016). KEGG enrichment statistics were computed with a hypergeometric test and was performed
480 separately for up- and down-regulated genes. Data from the transcriptome analysis of gacS mutant
481 were retrieved from supplementary table 3 in Cheng *et al.* (2013).

482

483 *Competition experiments*

484 SBW25 or SBW25-*lacZ* cell suspensions were spot-inoculated on separate KB agar plates and grown
485 for 7 days. Cells from the central ring were harvested, resuspended in Ringer's solution and gently
486 centrifuged to enrich suspensions in capsulated or non-capsulated cells. Capsulated SBW25 cells
487 were mixed with non-capsulated SBW-*lacZ* cells, and vice-versa. Mixed suspensions were diluted
488 100x in fresh KB and grown at 28°C in shaken tubes for 4h. Appropriate dilutions of the cultures
489 were plated on KB + X-gal plates at 0, 2h and 4h post-inoculation in order to measure the ratio of
490 white-blue colonies.

491

492 **Acknowledgements:**

493 The authors thank H. Hendrickson and P. Lind for help with microscopy and flow cytometry,
494 respectively, XX. Zhang for the generous gift of pUIC3-Δ*gacA* deletion plasmid, and E. Denisenko for
495 assistance with KEGG enrichment analyses. This work was supported in part by the Marsden Fund
496 Council and a James Cook Research Fellowship from government funding administered by the Royal
497 Society of New Zealand.

498

499

500 **Supplementary text: description of the mathematical model**

501 The protein PFLU3655 is a key regulator for capsulation; we assume that the amount of colanic acid
502 (and fluorescence from the P*pflu3655-GFP* reporter) produced by the cell is proportional to
503 PFLU3655 concentration, described by the variable *x*. The rate of change of *x* will be the result of
504 production, at rate P(x), and of degradation and dilution, whose rates can be for simplicity assumed
505 proportional to x. The time change of x will thus be described by the following ordinary differential
506 equation:

$$\frac{dx}{dt} = P(x) - dx$$

507 where the constant d measures the rate of degradation/dilution (or decay). The equilibrium
508 solutions of the system x_E are such that the production equalizes the decay, that is when $P(x_E)= d\ x_E$.
509 We can constrain the shape of the production P(x) term based on the experimental results.
510 PFLU3655 generates a positive feedback loop, meaning that P(x) is a positive function and the
511 production of the corresponding mRNA will be increasing with x (the more PFLU3655 protein, the
512 higher the production of mRNA). If there was no post-trancriptional regulation, the amount of mRNA
513 would determine the amount of protein produced, and P(x) would follow a Michealis-Menten
514 kinetics whose saturation value would be set by the concentration R of ribosomes (the higher the
515 concentration of ribosomes, the higher the maximal amount of protein that can be produced). In this
516 case, the system would be monostable and cells would be either on or off (x_E=0 or $x_E=x^{on}$), depending
517 on whether the baseline production is smaller or larger than the decay, respectively.

518 When protein production is regulated post-transcriptionally, however, the competition of RsmA/E
519 and ribosomes (whose concentrations are assumed to be constant) for binding to the mRNA can
520 produce an ultrasensitive dependence of P(x) on x (Fig. 5a; black line). For small x, the produced
521 *PFLU3655* mRNA will be almost entirely sequestered by RsmA/E and translation will be prevented.
522 Above a threshold concentration x_T, the titration by RsmA/E will be no longer sufficient to prevent
523 PFLU3655 proteins being produced, so that the production will be positive (but maybe insufficient to
524 overcome the decay term). If the affinity of RsmA/E is much stronger than that of ribosomes, the
525 shape of P(x) will be very nonlinear, with the production term being effectively zero for $x<x_T$. Finally,
526 for high x we expect production to saturate because of the finite amount of available ribosomes.

527 It is well known that ultrasensitivity can produce bistability (MUKHERJI *et al.* 2011; ZHANG *et al.* 2013;
528 FERRELL AND HA 2014). This is graphically illustrated in Fig. 5a: when the decay term (the slope of the
529 dashed red line) is sufficiently small, there will be three equilibrium solutions. Two of these solutions
530 are stable, corresponding to the OFF (x_E=0) and the ON ($x_E=x^{on}$) states, and one unstable ($x_E=x^S$). The

531 unstable solution separates the space of concentrations x in two domains: for all $x<x^S$, the
532 concentration will decrease and eventually approach the OFF state, for larger concentrations it will
533 converge to the ON state. The position of x^S, thus the extension of the basins of attraction of the two
534 stable equilibria, determines what is the probability that random fluctuations in the protein
535 concentration or in its production will lead the system to change equilibrium. For instance, the
536 probability to switch ON will be higher the smaller the value of x^S.

537 To examine what qualitative changes in the state of the system are expected following a variation in
538 its parameters, let us first imagine that for the WT strain in exponential phase of growth the decay
539 line lays just above the production curve (Fig. 5a; solid red line): cells will be almost exclusively in the
540 OFF state, even though rare large fluctuations in the protein concentration may lead them to be
541 'trapped' for some time in the region around the ON state. In the *carB* mutants, an increase in
542 ribosome concentration leads to an increase in the maximal production rate such that the two
543 curves cross in three points (Fig. 5b). There are now two alternative stable states, and the population
544 will contain a sizeable fraction of capsulated cells.

545 Changes in the parameters of the system can lead both to the transition from mono- to bistability
546 and to a change in the extent of the basins of attraction of the two stable equilibria, thus of the
547 population composition. When the baseline level of protein production is increased, as for instance
548 when the gene *PFLU3655* is inserted on a plasmid (Fig. 3b), the curve P(x) is displaced towards
549 higher values (Fig. 5c). This causes both the threshold concentration (thus the proportion of ON
550 cells) and the protein concentration (thus cell fluorescence) to increase.

551

552

553 **References:**

554 Ackermann, M., 2015 A functional perspective on phenotypic heterogeneity in microorganisms. Nat
555 Rev Microbiol 13: 497-508.
556 Bao, Y., D. P. Lies, H. Fu and G. P. Roberts, 1991 An improved Tn7-based system for the single-copy
557 insertion of cloned genes into chromosomes of gram-negative bacteria. Gene 109: 167-168.
558 Beaumont, H. J. E., J. Gallie, C. Kost, G. C. Ferguson and P. B. Rainey, 2009 Experimental evolution of
559 bet hedging. Nature 462: 90-U97.
560 Bodi, Z., Z. Farkas, D. Nevozhay, D. Kalapis, V. Lazar *et al.*, 2017 Phenotypic heterogeneity promotes
561 adaptive evolution. PLoS Biol 15: e2000644.
562 Bollenbach, T., S. Quan, R. Chait and R. Kishony, 2009 Nonoptimal microbial response to antibiotics
563 underlies suppressive drug interactions. Cell 139: 707-718.
564 Buchler, N. E., and F. R. Cross, 2009 Protein sequestration generates a flexible ultrasensitive
565 response in a genetic network. Mol Syst Biol 5: 272.
566 Buchler, N. E., and M. Louis, 2008 Molecular titration and ultrasensitivity in regulatory networks. J
567 Mol Biol 384: 1106-1119.
568 Cheng, X., I. de Bruijn, M. van der Voort, J. E. Loper and J. M. Raaijmakers, 2013 The Gac regulon of
569 Pseudomonas fluorescens SBW25. Environ Microbiol Rep 5: 608-619.
570 Choi, K. H., J. B. Gaynor, K. G. White, C. Lopez, C. M. Bosio *et al.*, 2005 A Tn7-based broad-range
571 bacterial cloning and expression system. Nat Methods 2: 443-448.
572 Condon, C., S. French, C. Squires and C. L. Squires, 1993 Depletion of functional ribosomal RNA
573 operons in Escherichia coli causes increased expression of the remaining intact copies.
574 EMBO J 12: 4305-4315.
575 Dennis, P. P., M. Ehrenberg and H. Bremer, 2004 Control of rRNA synthesis in Escherichia coli: a
576 systems biology approach. Microbiol Mol Biol Rev 68: 639-668.
577 Ehrenberg, M., H. Bremer and P. P. Dennis, 2013 Medium-dependent control of the bacterial growth
578 rate. Biochimie 95: 643-658.
579 Ellis, B., P. Haaland, F. Hahne, N. Le Meur, N. Gopalakrishnan *et al.*, 2017 flowCore: Basic structures
580 for flow cytometry data, R package version 1.44.0.
581 Farr, A. D., P. Remigi and P. B. Rainey, 2017 Adaptive evolution by spontaneous domain fusion and
582 protein relocalization. Nat Ecol Evol 1: 1562-1568.
583 Ferrell, J. E., Jr., and S. H. Ha, 2014 Ultrasensitivity part II: multisite phosphorylation, stoichiometric
584 inhibitors, and positive feedback. Trends Biochem Sci 39: 556-569.
585 Fridman, O., A. Goldberg, I. Ronin, N. Shoresh and N. Q. Balaban, 2014 Optimization of lag time
586 underlies antibiotic tolerance in evolved bacterial populations. Nature 513: 418-421.
587 Gallie, J., E. Libby, F. Bertels, P. Remigi, C. B. Jendresen *et al.*, 2015 Bistability in a metabolic network
588 underpins the de novo evolution of colony switching in Pseudomonas fluorescens. PLoS Biol
589 13: e1002109.
590 Gyorfy, Z., G. Draskovits, V. Vernyik, F. F. Blattner, T. Gaal *et al.*, 2015 Engineered ribosomal RNA
591 operon copy-number variants of E. coli reveal the evolutionary trade-offs shaping rRNA
592 operon number. Nucleic Acids Res 43: 1783-1794.
593 Heeb, S., C. Blumer and D. Haas, 2002 Regulatory RNA as mediator in GacA/RsmA-dependent global
594 control of exoproduct formation in Pseudomonas fluorescens CHA0. J Bacteriol 184: 1046-
595 1056.
596 Hindre, T., C. Knibbe, G. Beslon and D. Schneider, 2012 New insights into bacterial adaptation
597 through in vivo and in silico experimental evolution. Nat Rev Microbiol 10: 352-365.
598 Ho, S. N., H. D. Hunt, R. M. Horton, J. K. Pullen and L. R. Pease, 1989 Site-directed mutagenesis by
599 overlap extension using the polymerase chain reaction. Gene 77: 51-59.
600 Keener, J., and M. Nomura, 1996 Regulation of ribosome synthesis, pp. 1417-1431 in *Escherichia coli*
601 *and Salmonella: cellular and molecular biology*, edited by F. C. Neidhardt, R. Curtiss III, J. L.
602 Ingraham, E. C. C. Lin, K. B. Low *et al.* American Society for Microbiology, Washington, D.C.

603 Kim, W., S. B. Levy and K. R. Foster, 2016 Rapid radiation in bacteria leads to a division of labour. Nat
604 Commun 7: 10508.
605 Kim, W., F. Racimo, J. Schluter, S. B. Levy and K. R. Foster, 2014 Importance of positioning for
606 microbial evolution. Proc Natl Acad Sci U S A 111: E1639-1647.
607 King, E. O., M. K. Ward and D. E. Raney, 1954 Two simple media for the demonstration of pyocyanin
608 and fluorescin. J Lab Clin Med 44: 301-307.
609 Koch, A. L., 1971 The adaptive responses of Escherichia coli to a feast and famine existence. Adv
610 Microb Physiol 6: 147-217.
611 Lapouge, K., M. Schubert, F. H. Allain and D. Haas, 2008 Gac/Rsm signal transduction pathway of
612 gamma-proteobacteria: from RNA recognition to regulation of social behaviour. Mol
613 Microbiol 67: 241-253.
614 Mori, M., S. Schink, D. W. Erickson, U. Gerland and T. Hwa, 2017 Quantifying the benefit of a
615 proteome reserve in fluctuating environments. Nat Commun 8: 1225.
616 Mukherji, S., M. S. Ebert, G. X. Zheng, J. S. Tsang, P. A. Sharp *et al.*, 2011 MicroRNAs can generate
617 thresholds in target gene expression. Nat Genet 43: 854-859.
618 New, A. M., B. Cerulus, S. K. Govers, G. Perez-Samper, B. Zhu *et al.*, 2014 Different levels of
619 catabolite repression optimize growth in stable and variable environments. PLoS Biol 12:
620 e1001764.
621 Norman, T. M., N. D. Lord, J. Paulsson and R. Losick, 2015 Stochastic Switching of Cell Fate in
622 Microbes. Annu Rev Microbiol 69: 381-403.
623 Paul, B. J., W. Ross, T. Gaal and R. L. Gourse, 2004 rRNA transcription in Escherichia coli. Annu Rev
624 Genet 38: 749-770.
625 Rainey, P. B., 1999 Adaptation of Pseudomonas fluorescens to the plant rhizosphere. Environ
626 Microbiol 1: 243-257.
627 Rainey, P. B., P. Remigi, A. D. Farr and P. A. Lind, 2017 Darwin was right: where now for experimental
628 evolution? Curr Opin Genet Dev 47: 102-109.
629 Rendueles, O., M. Garcia-Garcera, B. Neron, M. Touchon and E. P. C. Rocha, 2017 Abundance and co-
630 occurrence of extracellular capsules increase environmental breadth: Implications for the
631 emergence of pathogens. PLoS Pathog 13: e1006525.
632 Richard, M., and G. Yvert, 2014 How does evolution tune biological noise? Front Genet 5: 374.
633 Roberts, I. S., 1996 The biochemistry and genetics of capsular polysaccharide production in bacteria.
634 Annu Rev Microbiol 50: 285-315.
635 Rotem, E., A. Loinger, I. Ronin, I. Levin-Reisman, C. Gabay *et al.*, 2010 Regulation of phenotypic
636 variability by a threshold-based mechanism underlies bacterial persistence. Proc Natl Acad
637 Sci U S A 107: 12541-12546.
638 Sambrook, J., E. F. Fritsch and T. Maniatis, 1989 *Molecular cloning: a laboratory manual*. Cold Spring
639 Harbor Laboratory, Cold Spring Harbor, N.Y.
640 Schindelin, J., I. Arganda-Carreras, E. Frise, V. Kaynig, M. Longair *et al.*, 2012 Fiji: an open-source
641 platform for biological-image analysis. Nat Methods 9: 676-682.
642 Stearns, S. C., 1992 *The evolution of life histories*. Oxford University Press, Oxford ; New York.
643 Vadia, S., and P. A. Levin, 2015 Growth rate and cell size: a re-examination of the growth law. Curr
644 Opin Microbiol 24: 96-103.
645 Vakulskas, C. A., A. H. Potts, P. Babitzke, B. M. Ahmer and T. Romeo, 2015 Regulation of bacterial
646 virulence by Csr (Rsm) systems. Microbiol Mol Biol Rev 79: 193-224.
647 Valentini, M., D. Gonzalez, D. A. Mavridou and A. Filloux, 2017 Lifestyle transitions and adaptive
648 pathogenesis of Pseudomonas aeruginosa. Curr Opin Microbiol 41: 15-20.
649 van Boxtel, C., J. H. van Heerden, N. Nordholt, P. Schmidt and F. J. Bruggeman, 2017 Taking chances
650 and making mistakes: non-genetic phenotypic heterogeneity and its consequences for
651 surviving in dynamic environments. J R Soc Interface 14.

652 Van den Bergh, B., J. E. Michiels, T. Wenseleers, E. M. Windels, P. V. Boer *et al.*, 2016 Frequency of
653 antibiotic application drives rapid evolutionary adaptation of Escherichia coli persistence.
654 Nat Microbiol 1**:** 16020.
655 Veening, J. W., W. K. Smits and O. P. Kuipers, 2008 Bistability, epigenetics, and bet-hedging in
656 bacteria. Annu Rev Microbiol 62**:** 193-210.
657 Zhang, Q., S. Bhattacharya and M. E. Andersen, 2013 Ultrasensitive response motifs: basic amplifiers
658 in molecular signalling networks. Open Biol 3**:** 130031.
659 Zhang, X. X., and P. B. Rainey, 2007 Construction and validation of a neutrally-marked strain of
660 Pseudomonas fluorescens SBW25. J Microbiol Methods 71**:** 78-81.

661

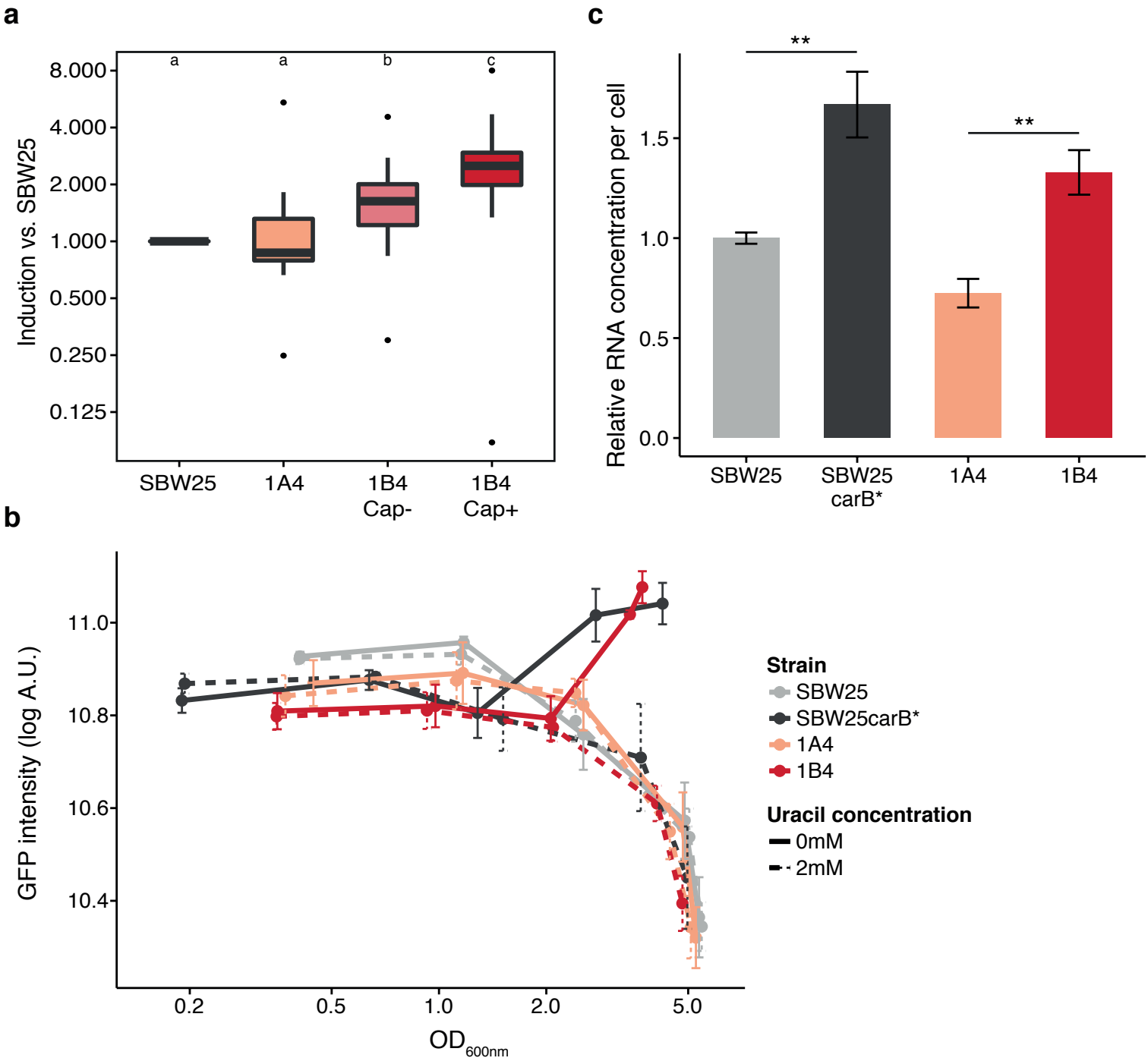

Figure 1: Increased ribosome production in *carB* mutants

a. Transcriptional induction of ribosomal protein genes in SBW25, 1A4, 1B4 Cap- and 1B4 Cap+ cells. Absolute expression levels of ribosomal protein genes (KEGG pathway '0310-Ribosomes', n=26) were extracted from a previous RNA-seq dataset (Gallie *et al.* 2015) and normalised to SBW25. Letter groups indicate statistical significance; $P < 0.05$, Kruskall-Wallis test with Dunn's post-hoc correction.

b. Expression kinetics of the P*rrnB*-GFP transcriptional reporter. Fluorescence in individual cells was measured by flow cytometry. Mean fluorescence values of bacterial populations are reported. Means ± standard deviation are shown, n=4. Data are representative of 3 independent experiments.

c. Total RNA concentration in bacterial cells during exponential phase (OD=0.5-0.6) normalized per cell count. Values were normalized to SBW25 control within each experiment. Means ± standard deviation are shown, n=6. ** $P<0.01$, Student's t-test.

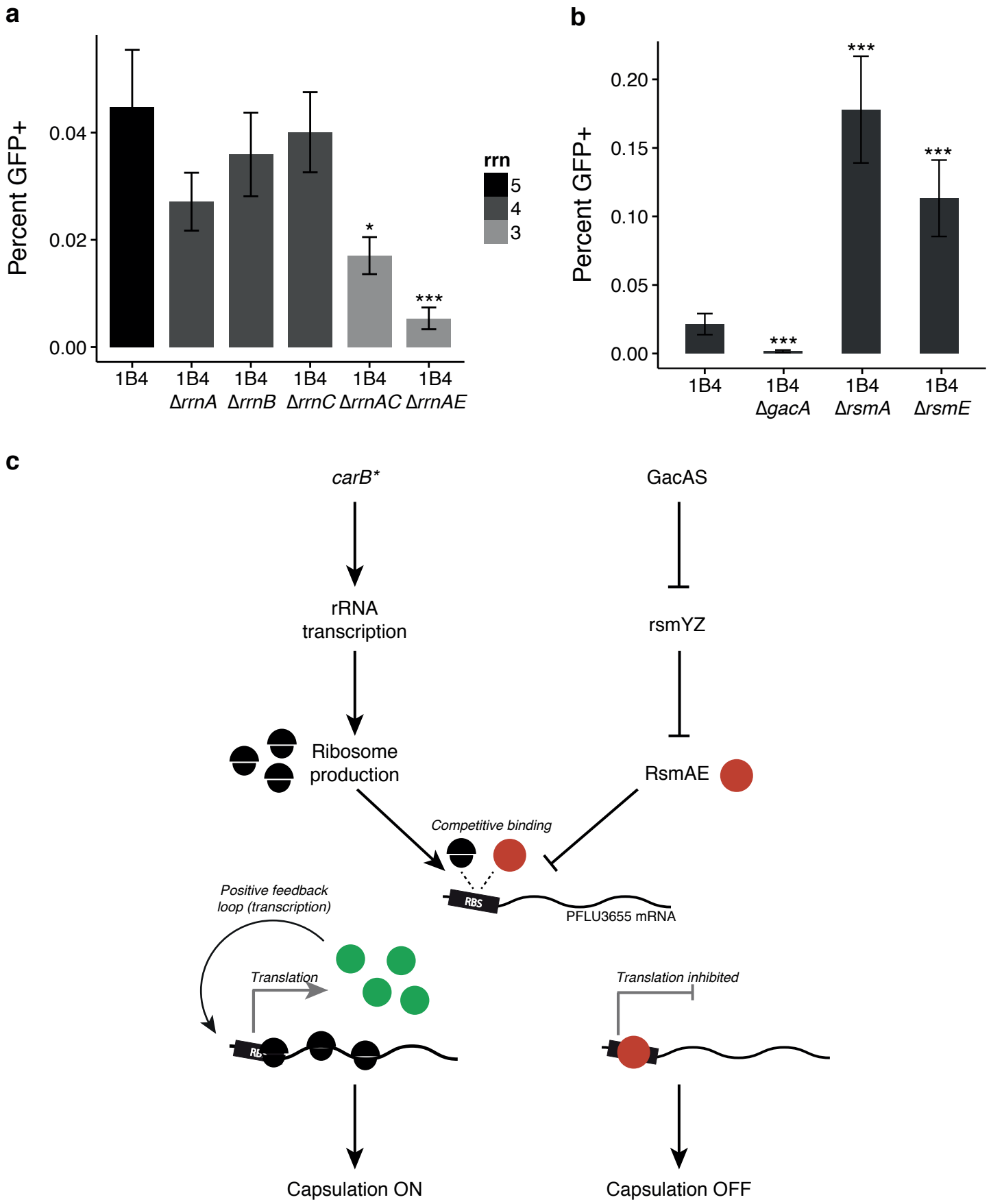

Figure 2: Genetic bases of capsulation

a. Capsulation in *rrn* deletion mutants.The Tn7-P*pflu3655*-GFP reporter was introduced in 1B4 bacteria ("WT") and its derived *rrn* mutants. Capsulation was measured by quantifying the proportion of GFP positive cells by flow cytometry at the onset of stationary phase (OD~2). Means ± standard error of the mean are shown, n≥8. Data were pooled from 4 independent experiments.* $P < 0.05$, *** $P < 0.001$, Dunn's test with Benjamini-Hochberg post-hoc correction, comparison to WT.

b. Capsulation in *gac*/*rsm* mutants. Means ± standard error of the mean are shown, n=9. Data are pooled from 3 independent experiments. *** $P < 0.001$, Dunnett's multiple comparison test on log-transformed data.

c. A model for capsulation in 1B4. See text for details.

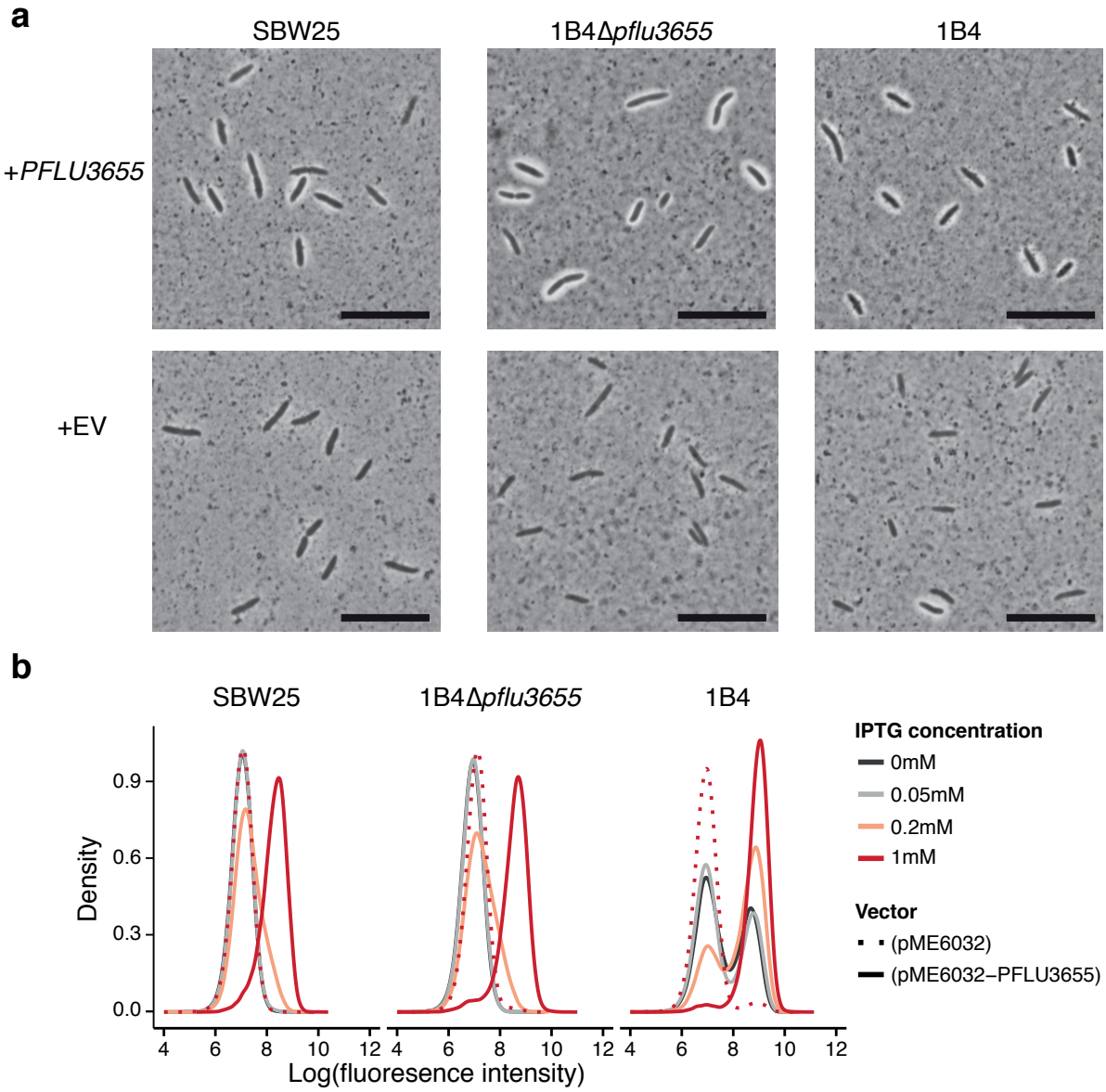

Figure 3: *PFLU3655* expression is necessary and sufficient for capsulation

a. Capsulation in SBW25, 1B4Δ*pflu3655* and 1B4 strains carrying the pME6032-*PFLU3655* plasmid or empty vector (EV) after induction with 1mM IPTG. Phase contrast microscopy images of bacterial suspensions counter-stained with indian ink. White halo around cells indicate capsulation. Scale bar = 10 µm.

b. PFLU3655 establishes a positive feedback loop. GFP fluorescence from the P*pflu3655*-GFP reporter in SBW25 (left), 1B4Δ*pflu3655* (middle) or 1B4 (right) cells carrying the pME6032-*PFLU3655* plasmid or empty vector. *PFLU3655* expression was induced with IPTG at indicated concentration and fluorescence was measured by flow cytometry. Smoothed fluorescence distributions are shown. Data are representative of 3 independent experiments.

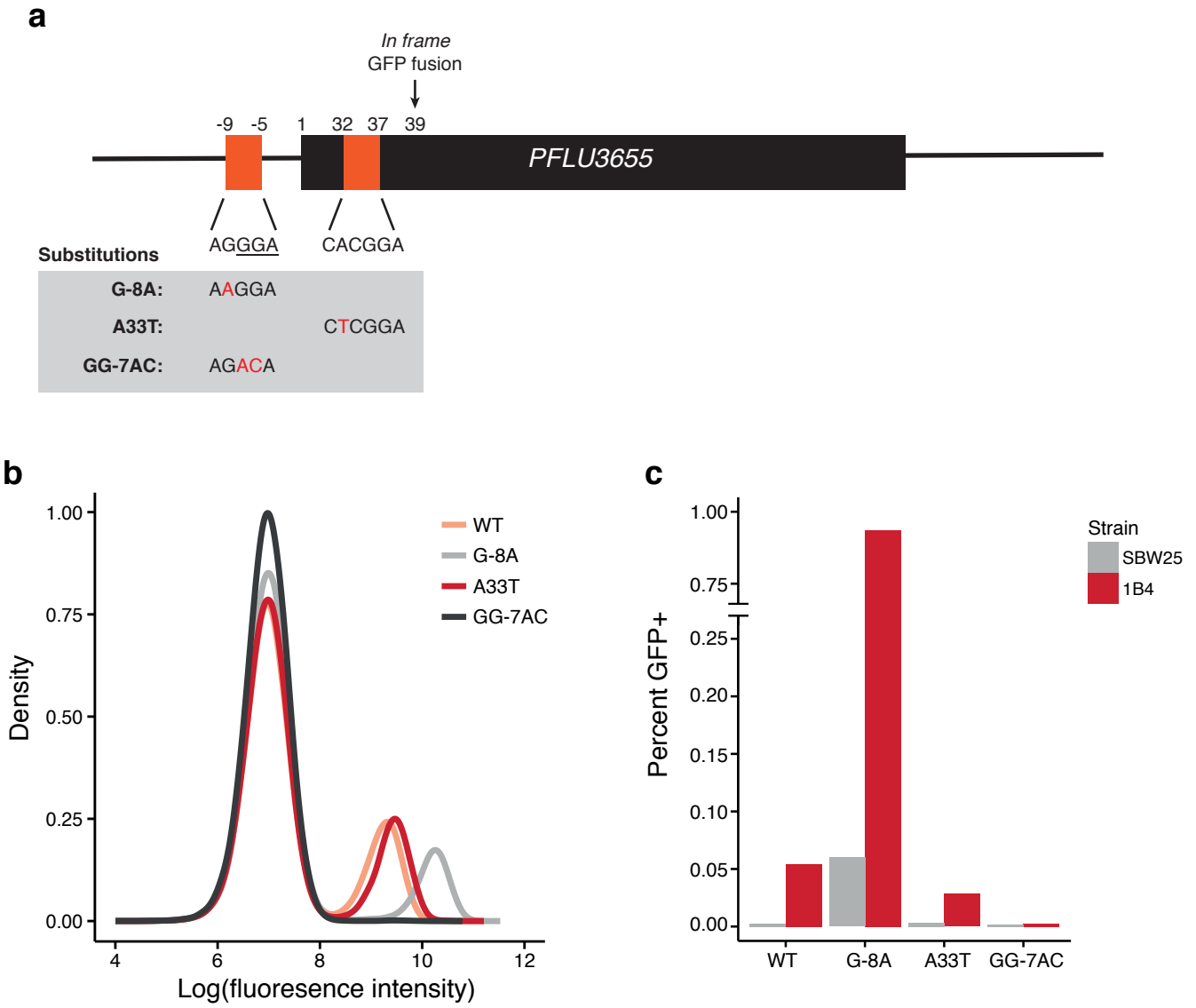

Figure 4: *PFLU3655* is a direct target of RsmA/E

a. Schematic diagram of *PFLU3655* region. Two putative RsmA/E binding sites (orange squares) are located in the promoter and 5' region of the gene. Numbers indicate nucleotide position relative to start codon (not to scale). Sequences of putative RsmA/E binding sites are shown, the putative ribosome-binding site (RBS) is underlined. Below: point mutations introduced in the different sequences by site-directed mutagenesis.

b. Expression of the P*pflu3655*-GFP reporter carrying the different point mutations in the 1B4 background. GFP fluorescence was measured by flow cytometry, smoothed distributions are shown. Data are representative of 3 independent experiments.

c. Mutations in putative RsmA/E binding sites affect capsulation. Individual point mutations were re-introduced into SBW25 and 1B4 carrying the wild-type P*pflu3655*-GFP reporter and the proportion of GFP positive cells in late exponential phase (OD~1-2) was measured by flow-cytometry.

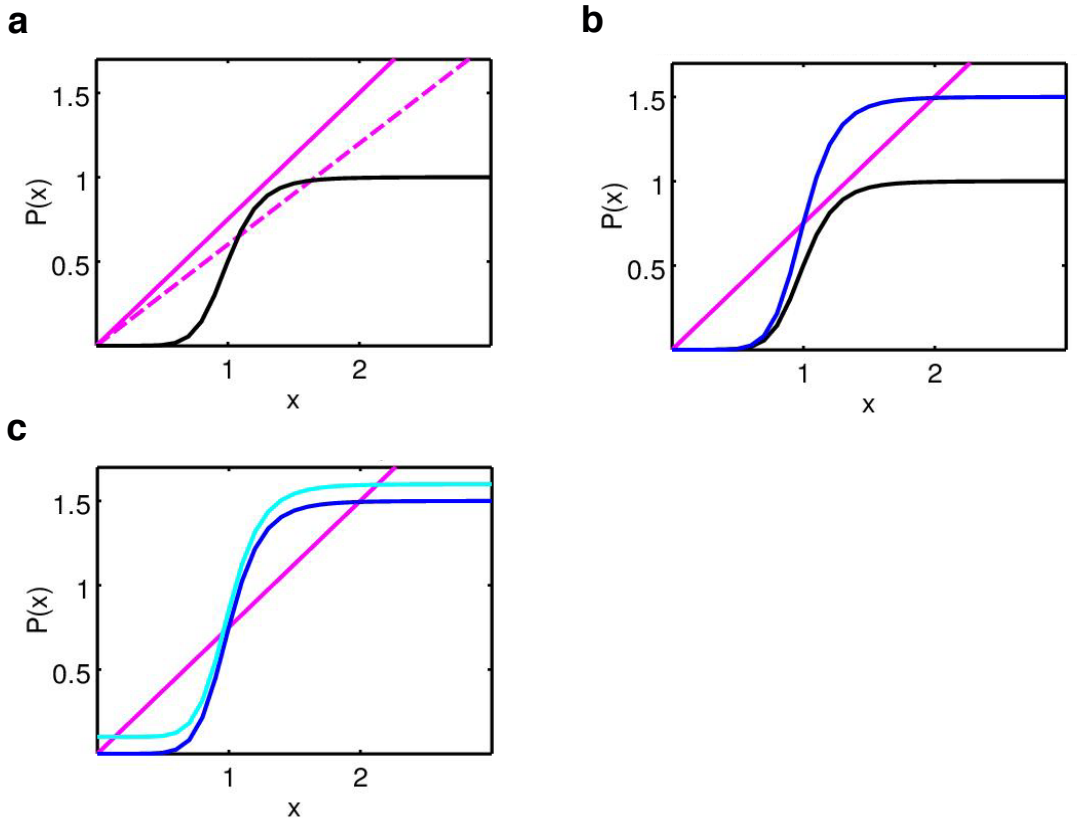

Figure 5: A mathematical model of capsulation allows to qualitatively explain switching behaviour

Graphical analysis of the effect of parameters on switching behaviour. Growth rate (a), ribosome concentration (b) and basal transcription rate of *PFLU3655* (c) can all affect the position of the equilibrium points.

Production curves P(x) are represented in black for wild-type SBW25 (a,b), in blue for *carB* mutants (b,c), and light blue for *carB* mutants with increased basal transcription of *PFLU3655* (c). Decay curves are drawn in purple. Stable or unstable equilibria are located at the intersections between production and decay curves.

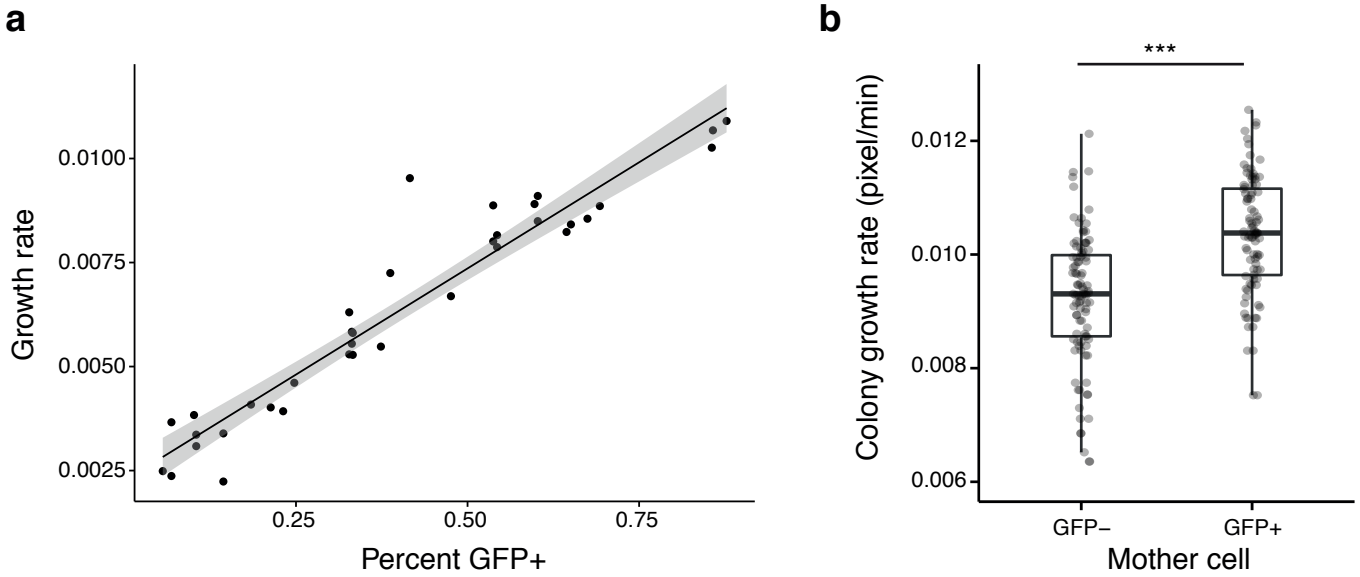

Figure 6: Capsulation and growth in 1B4

a. Initial growth rate after nutrient upshift depends on the proportion of capsulated cells in 1B4 populations. Data points pooled from 2 independent experiments. n=36, r^2=0.91. Shaded area indicates 95% confidence interval.

b. Growth rate of micro-colonies founded by cap- (GFP-) or cap+ (GFP+) cells measured by time-lapse microscopy. Growth rate was measured as the coefficient of the linear fit of the logarithm of colony area over time during the first 2h of growth. n=97 for GFP-; n=94 for GFP +. *** $P < 0.001$, Wilcoxon test.

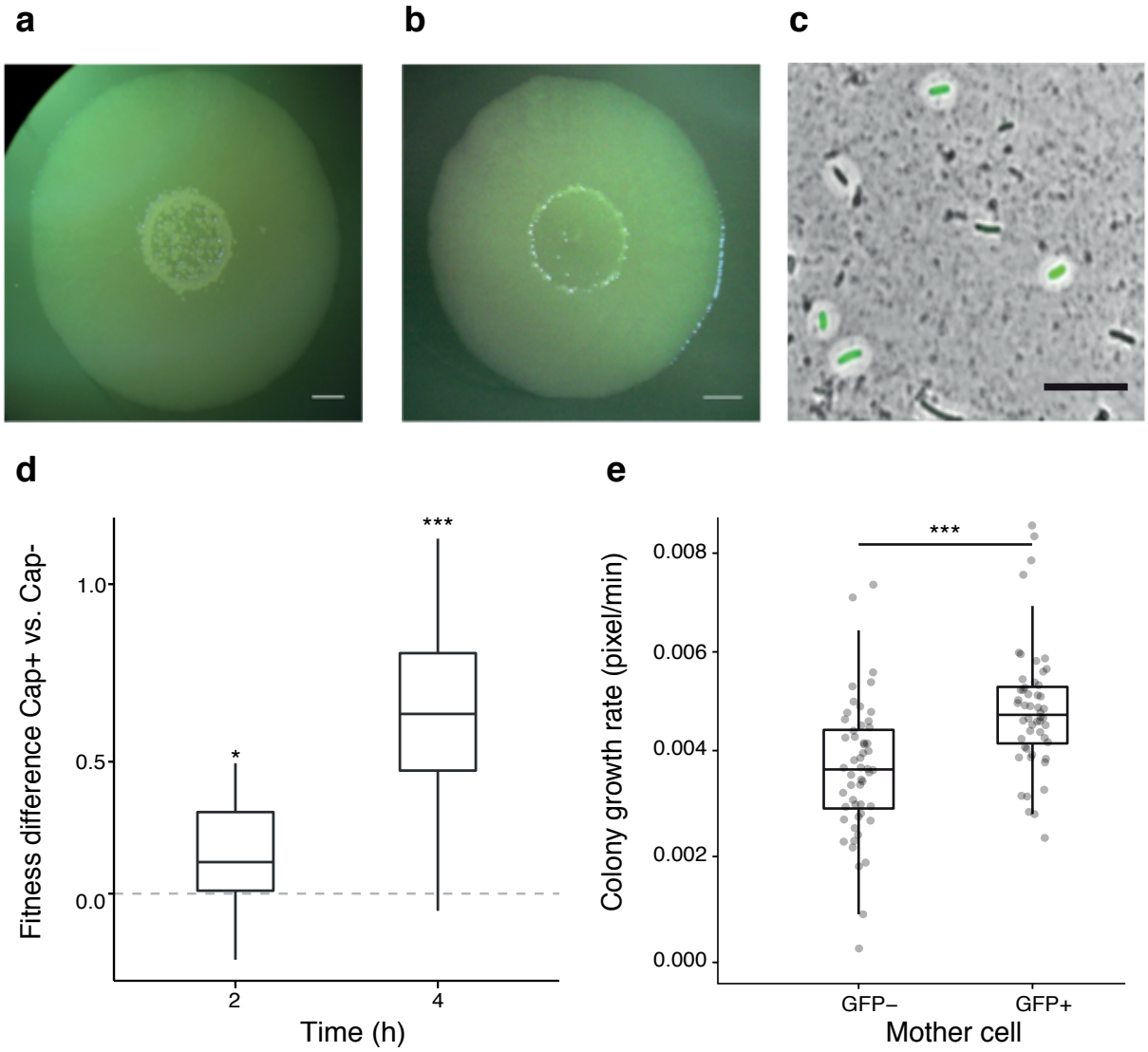

Figure 7: Capsulation and growth in SBW25

a-b. SBW25 colony grown on KB agar plate (a) or KB agar plate supplemented with 2mM uracil (b) for 7 days. Scale bar = 2 mm.

c. SBW25 cells carrying the Tn7-P*pflu3655*-GFP reporter and sampled from a 7-days old colony were counter-strained with indian ink to detect the presence of colanic-acid capsules. GFP images are overlaid to the phase contrast image. Scale bar = 10 µm.

d. Competitive fitness difference between SBW25 Cap- and Cap+ cells. Boxplot of he differences in Malthusian parameters between cultures enriched in Cap+ vs. Cap- cells are shown, n=12. * $P<0.05$, *** $P<0.001$, comparison to 0 with Student's t-test.

e. Growth rate of microcolonies founded by GFP- or GFP+ cells measured by time-lapse microscopy. Growth rate was measured as the first coefficient from the segmented fit of the logarithm of colony area over time during the first 2h of growth. n=65. *** $P < 0.001$, Wilcoxon test.

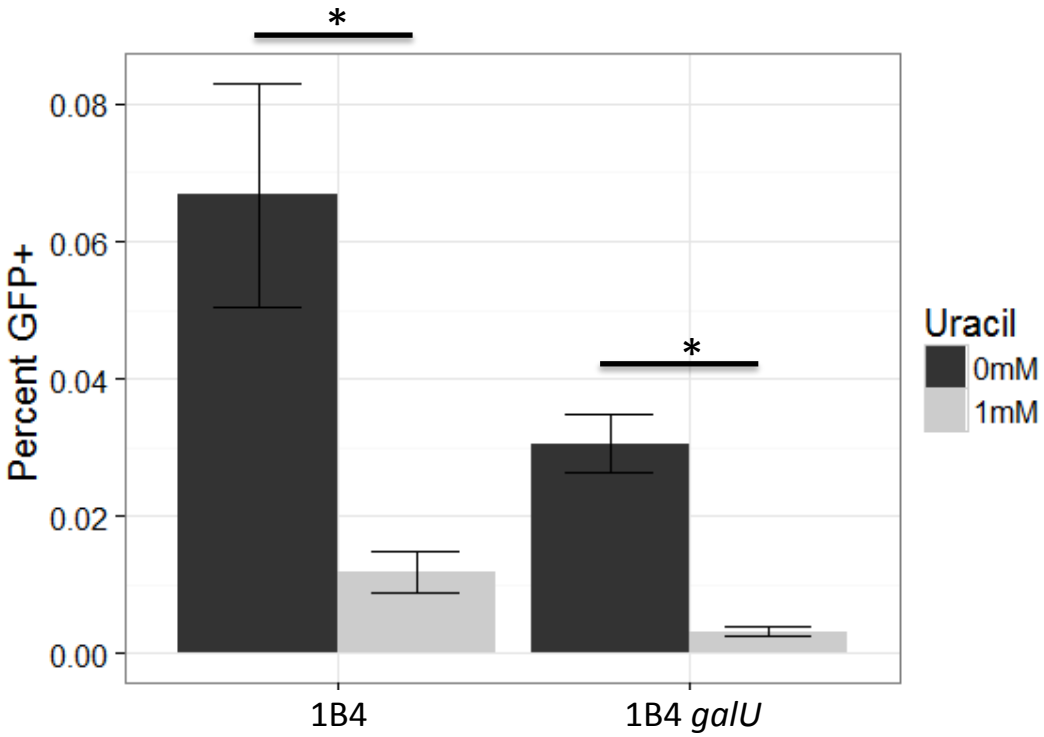

Supplementary Figure 1: Capsulation in the *galU* mutant

The Tn7-P*pflu3655*-GFP reporter was introduced in 1B4 and *galU* mutant. Capsulation was measured by quantifying the proportion of GFP positive cells by flow cytometry at the onset of stationary phase. Means ± standard deviation are shown. * $P < 0.05$, Student's t-test, n = 12.

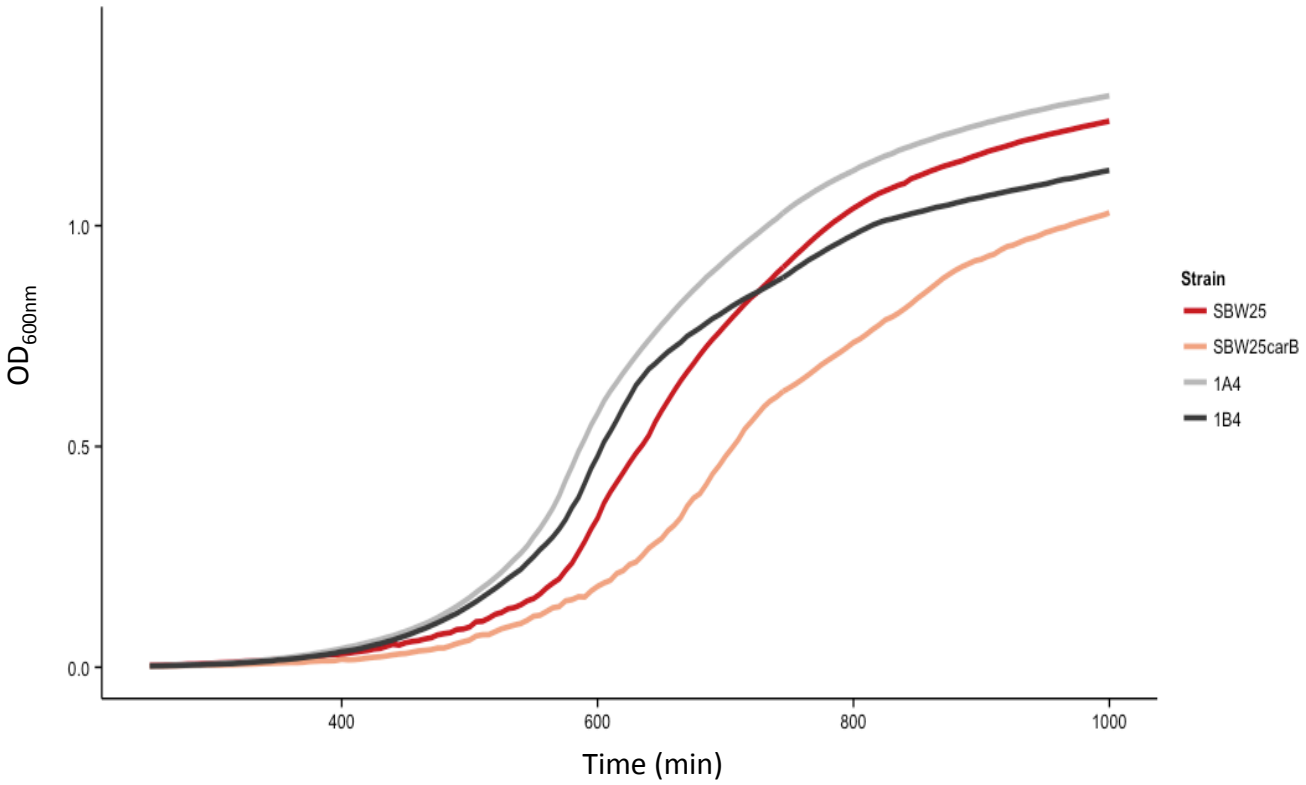

Supplementary Figure 2: Growth curves of *carB* mutants

Growth kinetics of SBW25, SBW25 *carB*, 1A4 and 1B4 strains in KB medium. Overnight cultures were diluted and used to inoculate 200µl KB cultures in a 96-well plate. OD_{600nm} was read in a microplate reader every 5min during incubation at 28°C with continuous shaking. Lines represent mean from 3 technical replicates.

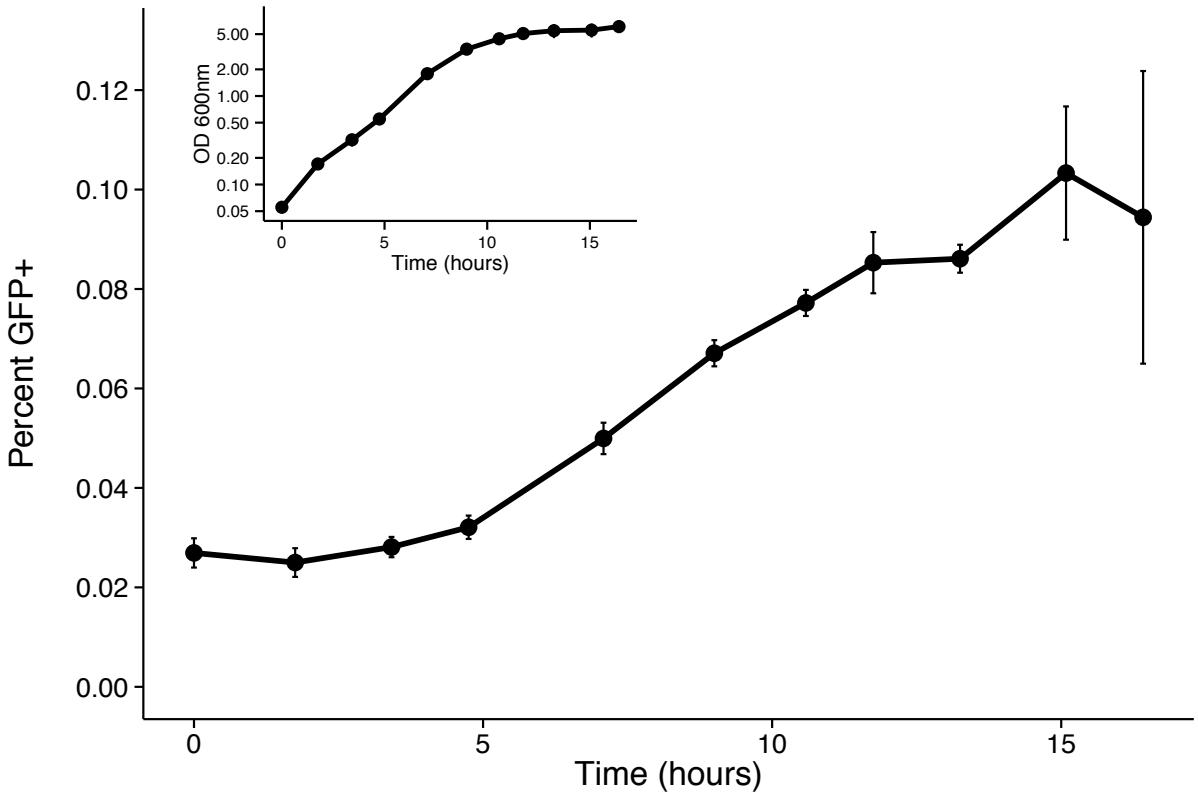

Supplementary figure 3: Capsulation kinetics in 1B4

The Tn7-P*pflu3655*-GFP reporter was introduced in 1B4. OD_{600nm} (inset) and the size of GFP positive subpopulation (main panel) were monitored over >15h. Capsulation was measured by quantifying the proportion of GFP positive cells by flow cytometry. Means ± standard deviation are shown, n=3. Data are representative of 2 independent experiments.

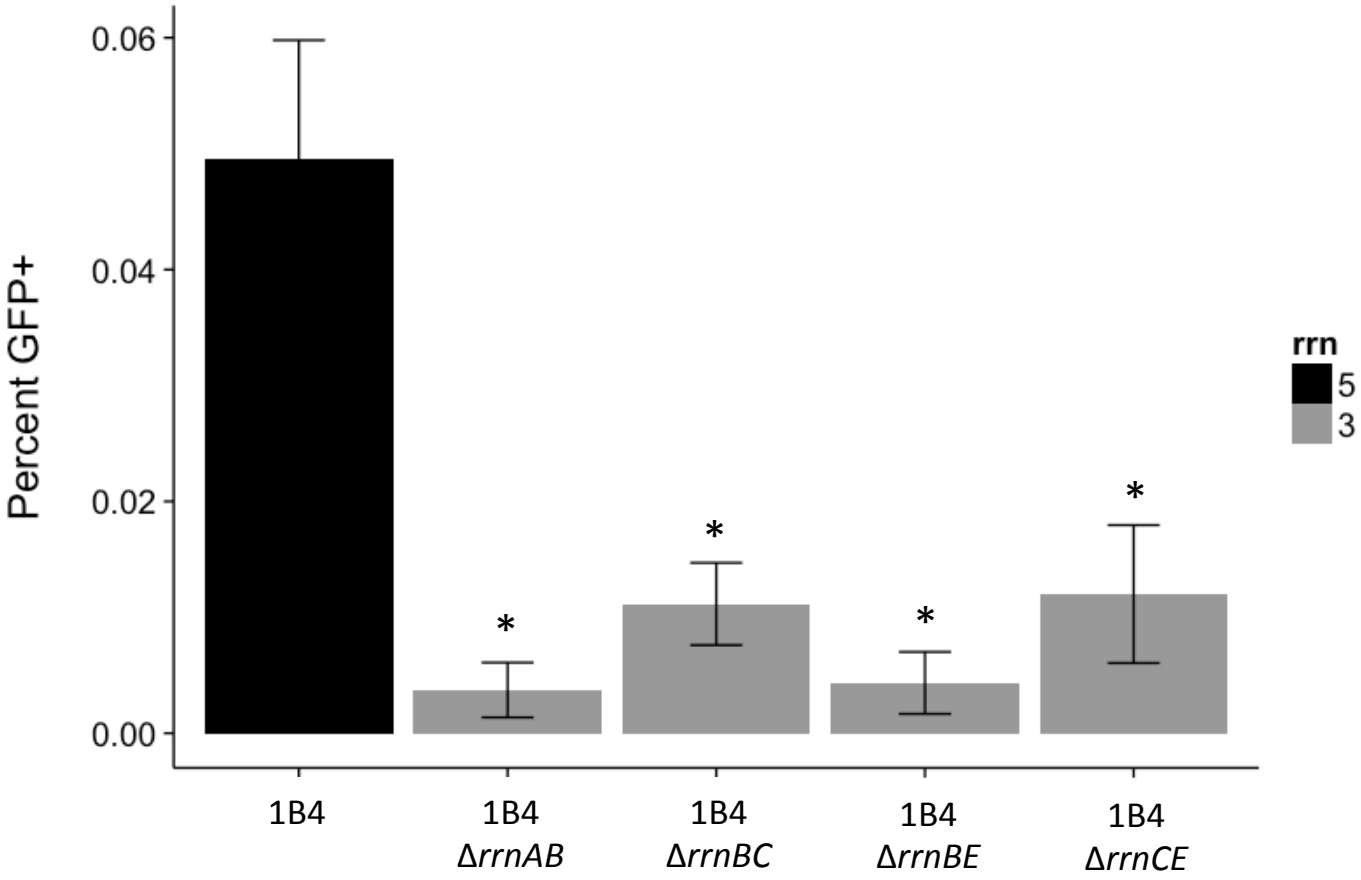

Supplementary Figure 4: Capsulation frequency in double *rrn* mutants
The Tn7-Pp*flu3655*-GFP reporter was introduced in 1B1 bacteria ("WT") and its derived *rrn* mutants. Capsulation was measured by quantifying the proportion of GFP positive cells by flow cytometry at the onset of stationary phase (OD~2). Color indicate the number of *rrn* operons per genotype. Means and standard error of the mean are shown, n≥9. Data are pooled from 3 independent experiments. * $P < 0.05$ compared to WT, Dunn's test with Benjamini-Hochberg post-hoc correction.

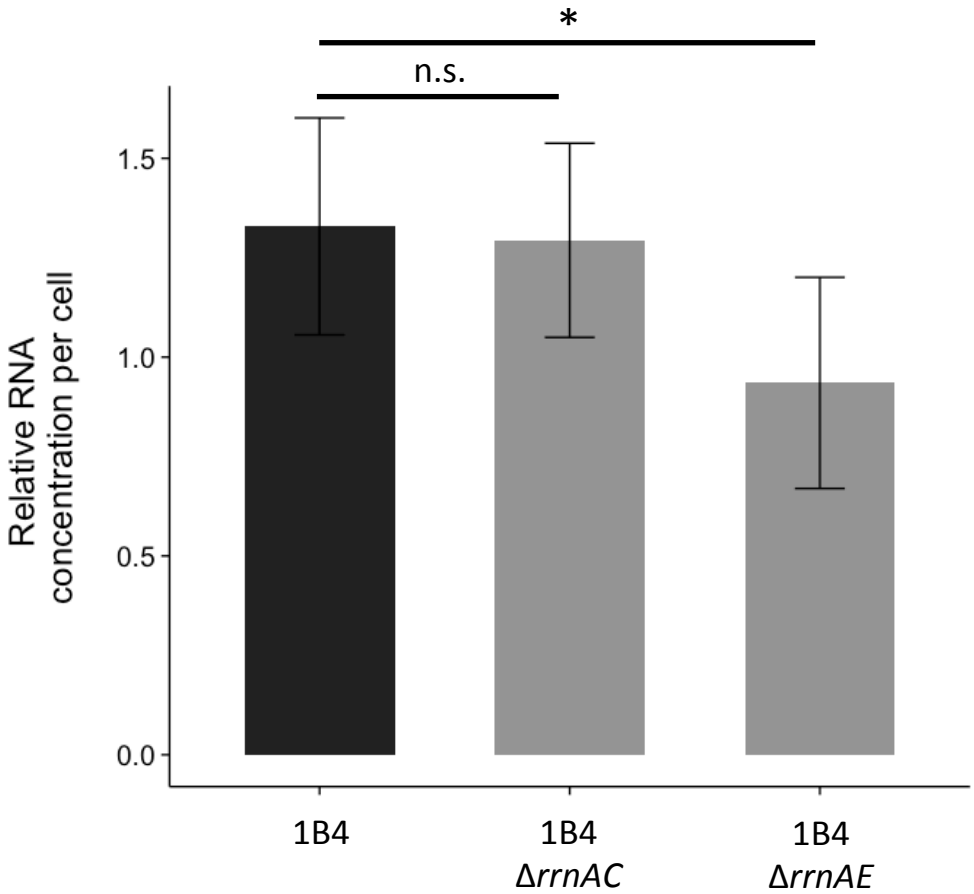

Supplementary Figure 5: RNA quantification in *rrn* mutants
Total RNA concentration in bacterial cells during exponential phase (OD=0.5-0.6) normalized per cell count. Values were normalized to SBW25 control within each experiment. Means ± standard deviation are shown, n=6. * $P<0.05$, Student's t-test. n.s. = not signifcant.

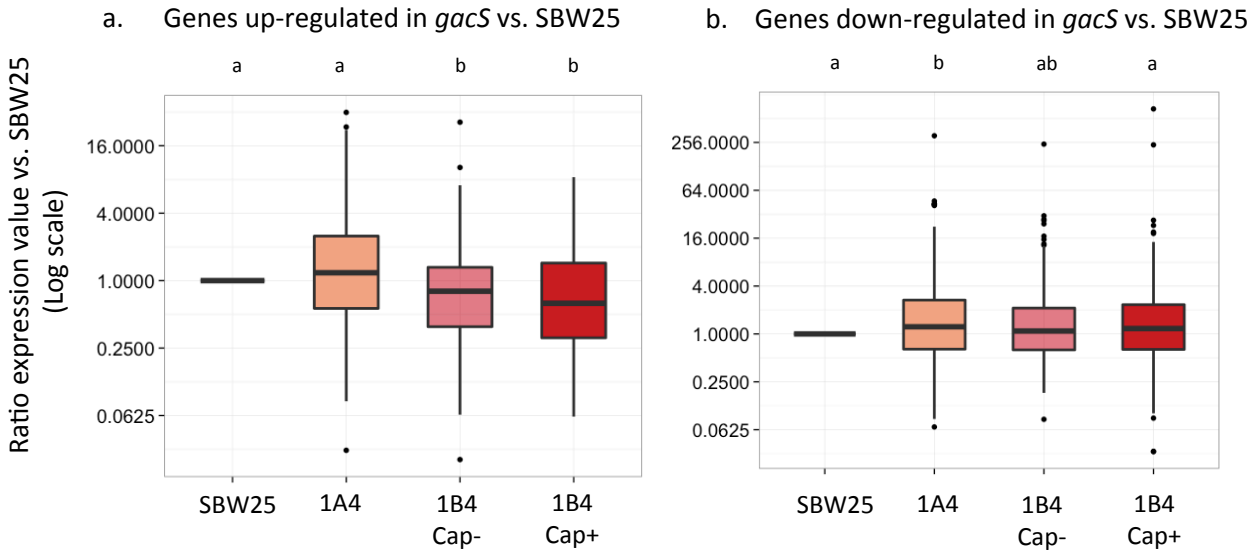

Supplementary figure 6: Expression of *gacS*-regulated genes

Genes that are up-regulated (left) or down-regulated (right) more than 4 times in a *gacS* mutant compared to WT SBW25 were recovered from Cheng *et al.* 2013 (dataset from supplementary table 3). The distribution of induction or repression values (after normalization by the base expression in SBW25) in the different RNAseq datasets is shown for each set of genes. n=125 (a) or 165 (b). Letter groups indicate statistical significance at $P < 0.05$, Kruskall-Wallis test with Dunn's post-hoc correction.

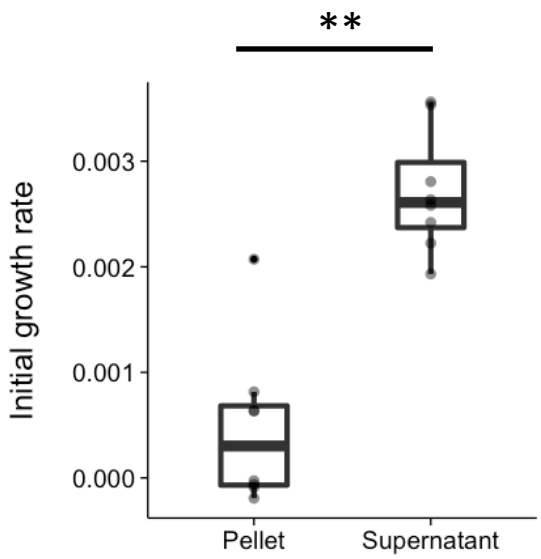

Supplementary Figure 7: Growth rate of SBW25 cultures enriched in Cap- or Cap+ cells

Cells from 7-day old colonies were resuspended in KB medium and suspensions were enriched in Cap- (pellet) or Cap+ (supernatant) cells by gentle centrifugation. The growth of these suspensions in a 96-well plate was measured with a microplate reader and the slopes from the fit of logarithm of density increase over time during the first 2h of growth are shown. n=8. ** $P < 0.01$, Wilcoxon test.